Effect of tantalum doping on the microstructure and photoelectrical properties of transparent conductive zinc oxide films
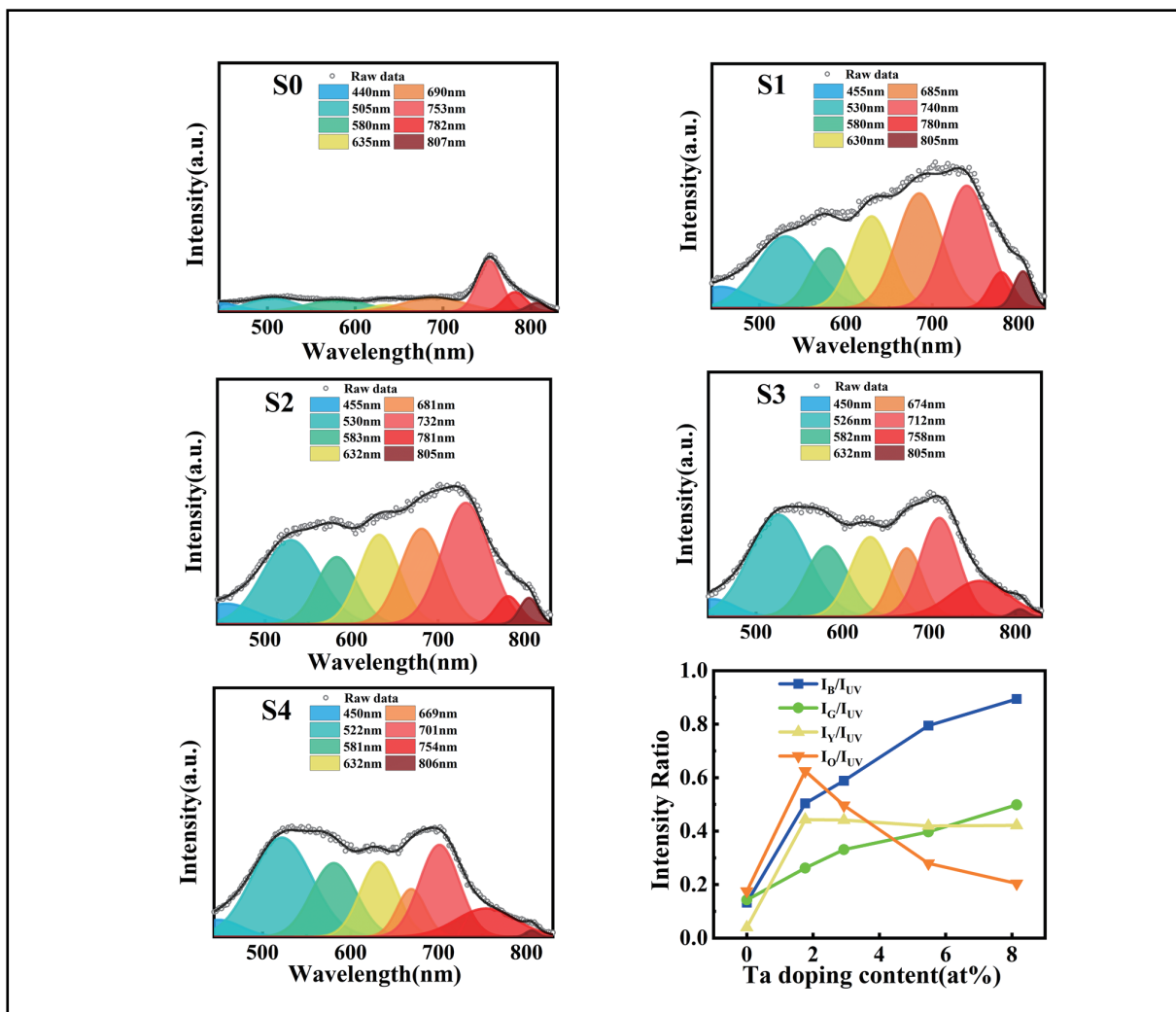
Kai Yi[1], Hongxu Jiang[1], Yanbo Cai[1], Guangwei Wang[1], Fei Liu[1], and Deliang Wang[1] ✉

[1]*Hefei National Laboratory for Physical Sciences at Microscale, University of Science and Technology of China, Hefei, Anhui 230026, China*

✉Correspondence: Deliang Wang, Email Address: eedewang@ustc.edu.cn

Graphical abstract

Public summary

- ■

- ■

- ■

Effect of tantalum doping on the microstructure and photoelectrical properties of transparent conductive zinc oxide films

Kai Yi[1], Hongxu Jiang[1], Yanbo Cai[1], Guangwei Wang[1], Fei Liu[1], and Deliang Wang[1] ✉

[1]*Hefei National Laboratory for Physical Sciences at Microscale, University of Science and Technology of China, Hefei, Anhui 230026, China*

✉Correspondence: Deliang Wang, Email Address: eedewang@ustc.edu.cn

Abstract: ZnO thin films with varying Ta concentrations were fabricated through magnetron sputtering. The crystallinity and surface morphology of the ZnO films are significantly influenced by the incorporation of Ta, as evidenced by the X-ray diffraction and scanning electron microscopy results. The lattice constants, as determined by X-ray diffraction, contradict the disparity in Ta and Zn ion radii, which is attributed to the impact of interstitial defects. This inconsistency introduces variations in carrier concentration in this experiment compared with prior studies. Subsequent exploration of the luminescent characteristics and emission mechanism of defect levels in Ta-doped ZnO films was conducted through photoluminescence. Furthermore, the factors influencing the bandgap are discussed.

Keywords: Tantalum-doped zinc oxide; RF magnetron sputtering; Microstructure; Photoluminescence

CLC number: **Document code: A**

Introduction

Considerable attention has been given to zinc oxide (ZnO) as an excellent n-type semiconductor because of its wide bandgap (3.37 eV), optical transparency, and large exciton binding energy (60 meV)[1]. Its applications span a range of fields, including photocatalysis, antibacterial materials, superhydrophobic coatings, gas sensors, solar cells, and diluted magnetic semiconductors[2–9]. Moreover, ZnO can also be applied in surface modification and to catalyze degradation processes[10,11]. Moreover, ZnO can be prepared through various straightforward techniques, including pulsed laser deposition, molecular beam epitaxy, spray pyrolysis, sol-gel and sputtering[12–19]. Typically, ZnO exhibits natural n-type conductivity, which is associated with the presence of shallow donor defects inside, such as oxygen vacancies and zinc interstitials[20].

The alteration of the luminescent behavior of ZnO can be caused by the introduction of various elements through doping. Generally, the photoluminescence of ZnO is divided into the ultraviolet region and the visible region. Ultraviolet emission is considered the characteristic emission of ZnO, attributed to near-band edge transition and exciton recombination[21]. Although visible region luminescence is widely believed to originate from internal defects, there is still controversy. Research has shown that doping different elements into ZnO allows flexible adjustment of its properties to meet the requirements of various fields. Doping is an important and widely used method in the optoelectronic field. The efficiency of doping is usually related to their electronegativity and the difference in ionic radii between the dopant and Zn ions[22]. The ionic radius of Ta^{5+} (0.064 nm) is not significantly different from that of Zn^{2+} (0.074 nm)[23]. Theoretically, Ta can replace Zn in the ZnO lattice without distorting the

crystal structure. There is a significant difference in the valence states between Ta^{5+} and Zn^{2+}. Therefore, even a small amount of doping can provide sufficient carriers. However, there are few reports in the literature concerning Ta-doped ZnO films[22–24]. Moreover, to the best of our knowledge, many characteristics of Ta-doped ZnO films, such as luminescence, have not been systematically studied. In this work, ZnO films with different Ta doping concentrations were prepared by magnetron sputtering, and the composition, morphology, microstructure and photoelectric properties of the Ta-doped ZnO films were studied.

Materials and methods

Ta-doped ZnO films were deposited in a multitarget magnetron sputtering system. Sputtering was carried out at room temperature using a ZnO target (99.99%) and a Ta_2O_5 target (99.99%). The deposition atmosphere was a mixture of 6% oxygen and 94% argon while maintaining a pressure of approximately 0.6 Pa during deposition. The sputtering power for the ZnO target was set at 60 W. The doping level of Ta was controlled by adjusting the sputtering power for the Ta_2O_5 target. The samples were labeled as follows: pure ZnO films without Ta doping were labeled S0, and the samples with Ta_2O_5 sputtering powers of 30, 35, 40, and 50 W were labeled S1, S2, S3, and S4, respectively. The deposition time was adjusted to achieve a film thickness of approximately 200 nm for all the samples. After deposition, the films were annealed in a tube furnace under a nitrogen atmosphere at a pressure of 10 Pa for 30 minutes.

The surface morphology and film thickness were investigated using a field emission scanning electron microscope (SEM, FEI Apreo). Concurrently, the composition of the

films was analyzed utilizing an energy dispersive spectroscopy system (EDS, Bruker X Flash 6130). To characterize the crystalline microstructure of the films, X-ray diffraction (XRD, MiniFlex 600) employing Cu Kα radiation was used. The surface properties and the valence state of the elements were assessed by means of X-ray photoelectron spectroscopy (XPS, Thermo Scientific ESCALAB 250Xi). The transmittance spectra of the films were measured using an Ultraviolet-visible spectrophotometer (Solid 3700 DUV). To evaluate the electrical properties of the film, the van der Pauw method was employed, and measurements were carried out using a Hall effect system set up in our laboratory. At room temperature, photoluminescence spectra were recorded using a high-resolution spectrometer (LabRAM HR Evolution) at wavelengths of 325, 473, and 532 nm lasers, respectively.

Results and Discussion

Due to the close proximity of the characteristic peak positions of Ta Mα (1.71 keV) and Si Kα (1.74 keV), the samples measured via EDS were grown on sapphire (Al_2O_3) substrates to prevent overlap of the characteristic peaks. The relationship between the sputtering power for the Ta_2O_5 target and the Ta content, as determined by EDS analysis, is depicted in Fig. 1. Since the mapping images did not reveal discernible variations, they have been omitted. The detailed surface morphology of the thin films is shown in Fig. 4. The atomic ratio of Ta/(Ta+Zn) in the films was calculated.

Sample S0 represents a pure ZnO film, whereas samples S1, S2, S3, and S4 have Ta contents of 1.8 at%, 2.9 at%, 5.5 at%, and 8.1 at%, respectively. The Ta content in the films gradually increased as the Ta_2O_5 sputtering power increased with a fixed ZnO sputtering power.

XPS measurements were performed to ascertain the chemical states of the elements, and the XPS spectra are displayed in Fig. 2. From the full spectrum, it is discernible that the deposited film is predominantly composed of Zn, Ta, O, and C, with the presence of C attributed to the adsorption of CO_2 from ambient air. In Fig. 2(b), the Zn core levels are located at symmetric peaks at 1021.7 eV and 1044.9 eV, corresponding to the $2p_{3/2}$ and $2p_{1/2}$ levels of Zn, with a spin-orbit splitting of 23.2 eV. These values closely align with the standard values observed in ZnO, suggesting that the majority of the Zn in the films exists in the form of Zn^{2+}[25]. Fig. 2(c) presents the 4f core level spectrum of Ta, featuring characteristic peaks at approximately 26.2 eV and 28.1 eV. According to prior literature, for the typical Ta^{5+} oxidation state, the Ta $4f_{7/2}$ and Ta $4f_{5/2}$ peaks are positioned at 26.8 eV and 28.7 eV, respectively[26]. For the Ta^{4+} oxidation state, the two peak positions are located at 25.1 eV and 27.2 eV[27]. In our experimental measurements, the binding energy positions of Ta $4f_{7/2}$ and Ta $4f_{5/2}$ fall between those of Ta^{5+} and Ta^{4+}, indicating that the measured Ta characteristic peaks result from the overlap of Ta^{5+} and Ta^{4+} peaks. This suggests the coexistence of Ta in that Ta coexists with both Ta^{5+} and Ta^{4+} in the film.
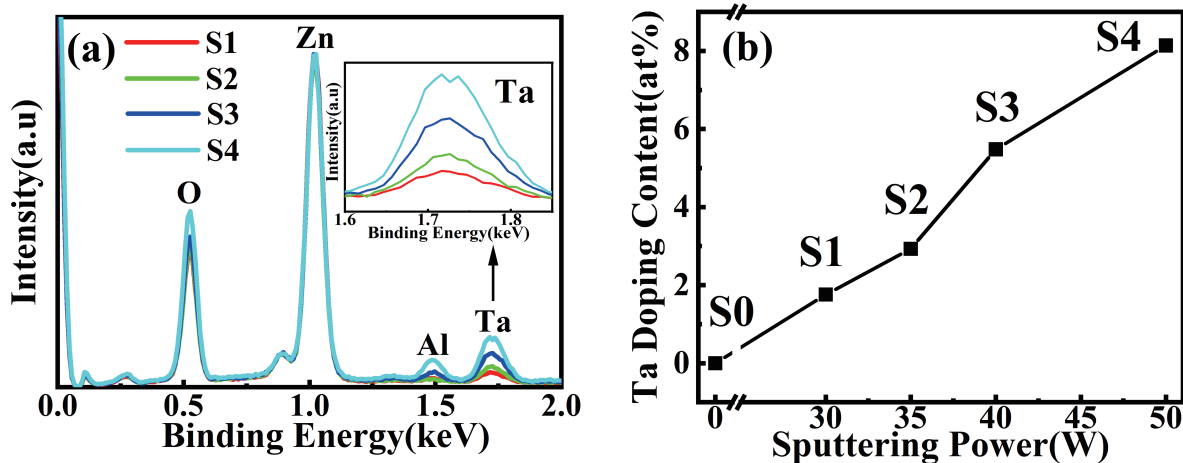

Fig. 1. (a) EDS of Ta-doped ZnO thin films; (b) relationship between Ta content and sputtering power.
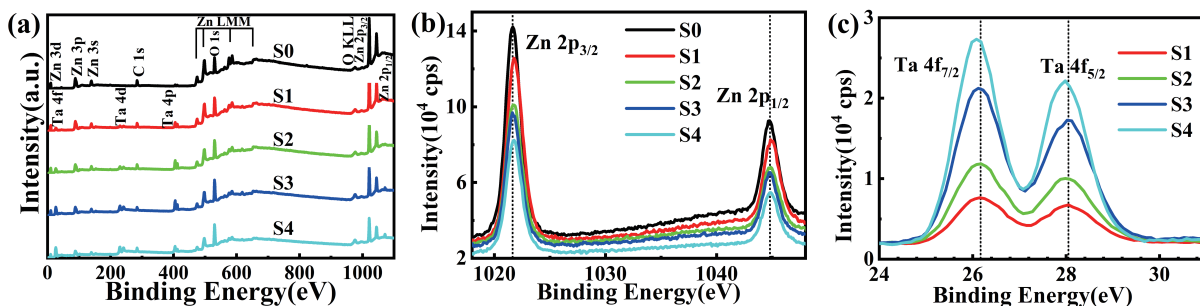

Fig. 2. XPS spectra of Ta-doped ZnO thin films: (a) full spectrum; (b) Zn 2p peak; (c) Ta 4f peak.

Microstructure

The XRD spectra of the undoped and Ta-doped ZnO films are presented in Fig. 3(a). It is evident that only one (002) diffraction peak is exhibited by all the samples, aligning with the hexagonal wurtzite ZnO standard pattern and is indicative of a high c-axis preferential orientation. Additionally, a noticeable shift of the diffraction peak toward lower angles is observed as the doping level increases, with the 2θ shifting from 34.26° to 33.34°. Simultaneously, there is a decrease in the intensity of the (002) diffraction peak, signifying the successful integration of the dopant into the ZnO films[28]. It is apparent that the inclusion of Ta does not result in the emergence of any additional phases within the films. Consequently, the crystal structure remains unaltered upon doping with Ta, suggesting the potential for Ta to replace Zn in lattices or be inserted at interstitial sites[29]. Furthermore, it was determined that the distinctive peak of (002) exhibited a discernible shift toward lower angles by calculating the lattice spacing using the Bragg diffraction equation $2d\sin\theta = n\lambda$. This phenomenon is conventionally attributed to the substitution of Zn^{2+} with larger doping ions[30]. However, it is noteworthy that the ionic radii of Ta^{5+} (0.064 nm), Ta^{4+} (0.068 nm), and Ta^{3+} (0.072 nm) are comparatively smaller than that of Zn^{2+} (0.074 nm)[23]. Thus, the explanation for this observation cannot be exclusively grounded in ionic radii considerations. Similar results have been reported for ZnO doped with Zr^{4+} (0.059 nm) and Mo^{6+} (0.041 nm), suggesting the involvement of additional defects linked to interstitial atoms and the dopant[31,32]. If all the doped Ta atoms were to occupy Zn sites, this would lead to a reduction in the lattice parameter. Consequently, the introduced Ta may partially enter the grain boundaries or interstitial sites, concurrently introducing additional defects. Notably, the standard lattice parameter c of ZnO is 5.206 Å, whereas that of the pure ZnO prepared in this experiment is 5.235 Å, which is greater than the standard value. This slight deviation implies the presence of inherent defects, including oxygen vacancies and interstitial atoms, in the ZnO films prepared via magnetron sputtering[33]. Upon Ta doping into ZnO, a swift reduction in the intensity of the diffraction peak and an increase in the FWHM of the peaks were observed. Analysis using the Scherrer equation revealed a reduction in the grain size, suggesting that the incorporation of Ta inhibited the growth of the ZnO microcrystals. Consequently, the doping of Ta resulted in a decrease in the crystallinity of the films. The SEM image of the film is shown in Fig. 4, and the Ta doping concentration has a significant effect on the surface morphology of ZnO. The undoped ZnO grains exhibit regular spherical shapes with relatively large grain sizes. Following a minor increase in doping, a decrease in the grain size is observed, with small grains aggregating to generate irregular large clusters. With a high doping concentration, the occurrence of grain aggregation diminishes, accompanied by an increase in the disorder of the film.

Hall measurements conducted on the films revealed that the carrier concentration of undoped ZnO and films with low Ta doping concentrations remained at approximately 10^{19} cm^{-3}. In previous studies, a minor amount of Ta doping was identified as increasing the carrier concentration by substituting Ta^{5+} for Zn^{2+} and supplying additional electrons. However, in this experiment, the introduction of Ta doping resulted in a deterioration of crystallinity, leading to the absence of a significant increase in the carrier concentration. This divergence from prior studies can be ascribed to variations in film preparation techniques, potentially diminishing the efficacy of doping[24,34]. Through the integration of XRD analysis, a reasonable speculation arises that partially doped Ta ions replace Zn sites in the lattice as donor defects, providing electrons. Another fraction may aggregate at grain boundaries or interstitial sites, forming positive defects that serve as electron traps, thereby restricting carriers, and both factors mutually constrain each other[35]. The decrease in carrier concentration after high-concentration Ta doping is related to the solubility of Ta in ZnO. The increased presence of Ta in interstitial spaces or at grain boundaries further reduces the carrier concentration. Mobility decreases with increasing Ta concentration, which is attributed to the aggregation of dopants and an increase in defects, consequently resulting in an increase in ionized scattering. Furthermore, the decrease in crystallinity contributes to increased grain boundary scattering, collectively impeding the migration of carriers.

Photoluminescence

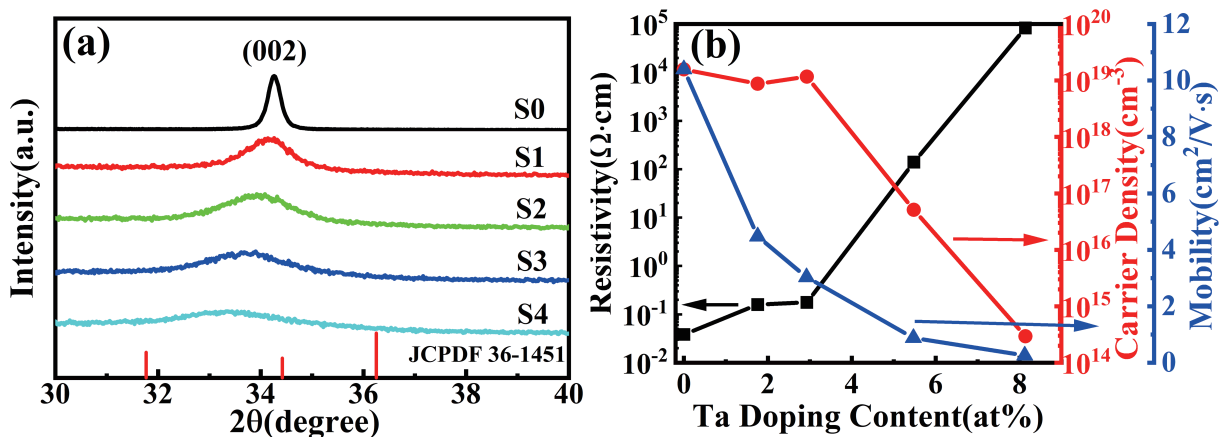To attain a better understanding of the alterations in the elec-

Fig. 3. (a) XRD of Ta-doped ZnO thin films; (b) relationships between the Ta content and the resistivity, carrier density, and mobility.

trical properties of thin films, a meticulous investigation of defect states is imperative. Photoluminescence serves as a common methodology for studying the luminescent characteristics, bandgap features, and point defects inherent in materials. The photoluminescence spectra of the films deposited on silicon substrates illuminated by excitation wavelengths of

532, 473, and 325 nm are shown in Fig. 5. Under 325 nm laser excitation, sharp ultraviolet (UV) region emission and broad visible light emission are observed in the sample. The UV emission is attributed primarily to near band edge (NBE) emission resulting from exciton recombination. A discernible shift of the UV emission peak toward shorter wavelengths oc-
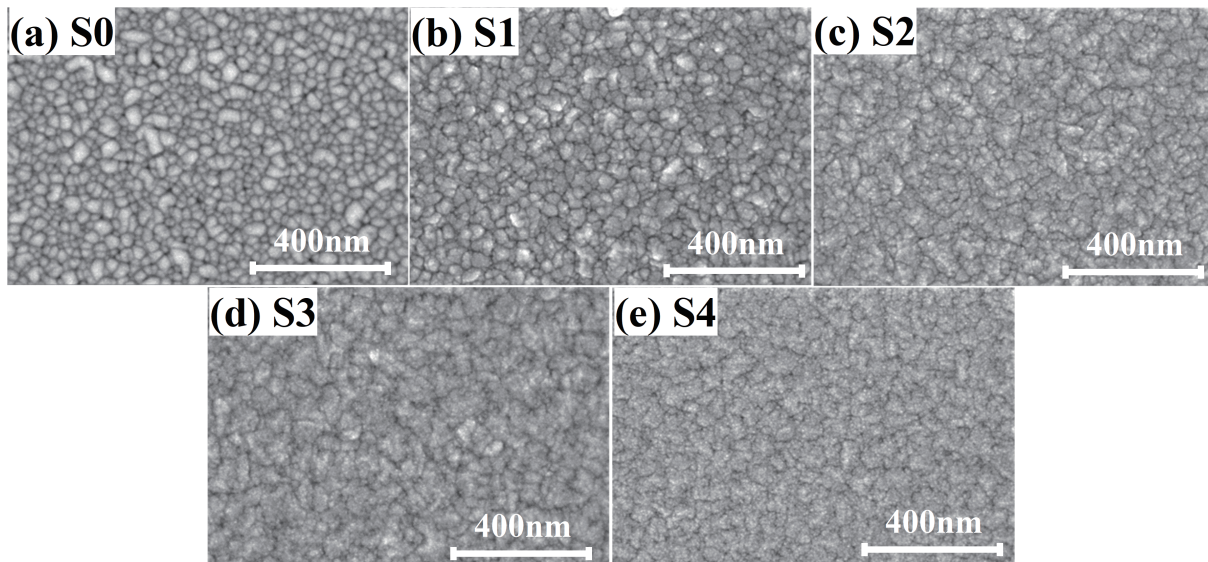

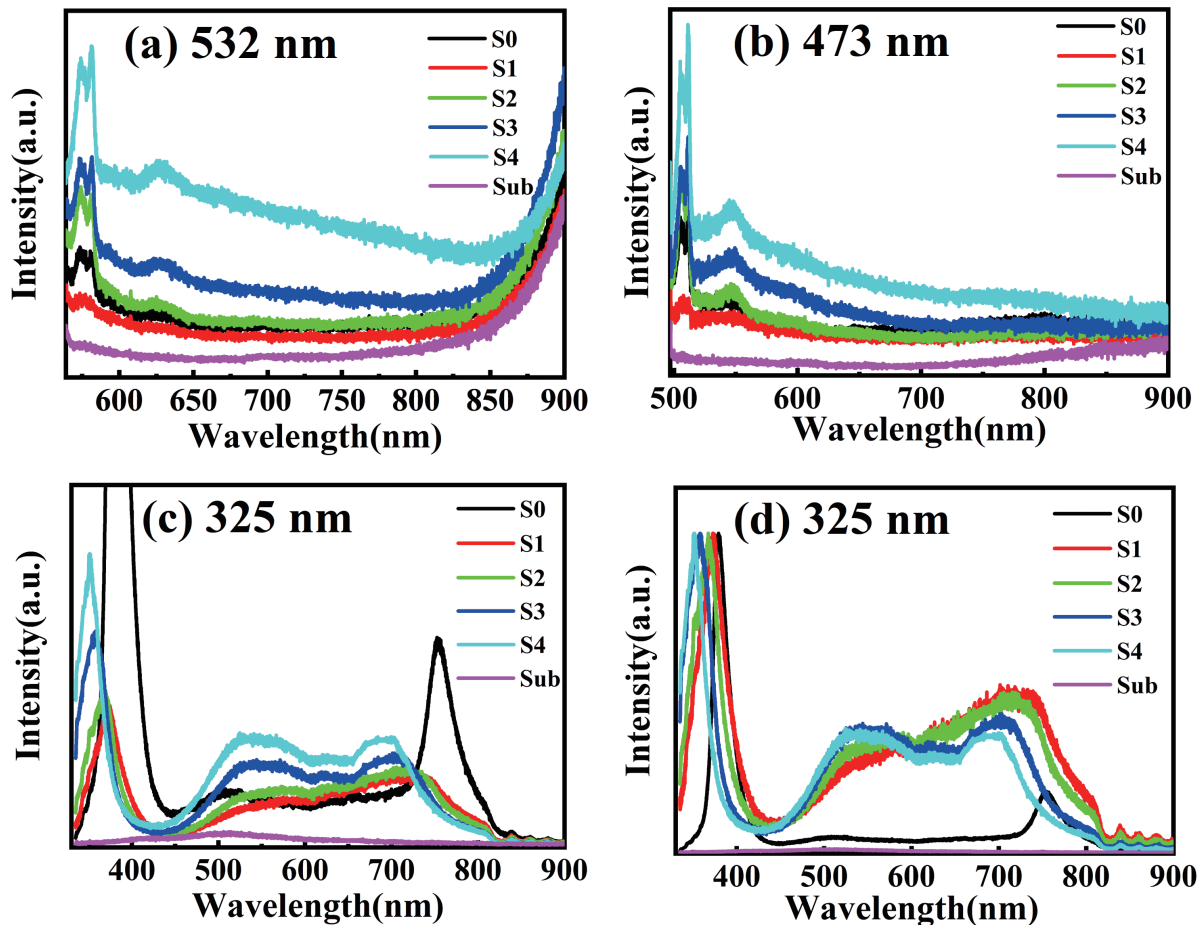**Fig. 4.** Surface morphology of ZnO thin films with different Ta contents.

Fig. 5. PL spectra of samples and substrates at different excitation wavelengths: (a) 532 nm, (b) 473 nm, (c) 325 nm, and (d) normalized PL spectrum of (c).

curs with increasing Ta doping concentration, reflecting an increase in the bandgap. The visible light emission is associated mainly with the defect energy levels within the films, such as zinc interstitials (Zn_i), extended zinc interstitials (ex-Zn_i), zinc vacancies (V_{Zn}), oxygen interstitials (O_i), and oxygen vacancies (V_O)[36]. The consistent trend in the absolute luminescence intensity variation across samples under diverse laser excitation wavelengths is evident. This phenomenon is attributed to the luminescent efficiency of the samples, a characteristic that may be intricately connected to the morphology and microstructure of the samples. Under the excitation of a 325 nm laser, a small peak is consistently observed, which aligns with approximately half of the NBE energy. The trend of changes in peak position aligns consistently with that of NBE. Moreover, under the excitation of 473 and 532 nm lasers, the disappearance of this peak suggests that it is not caused by intrinsic defects but rather the result of the second-order diffraction of ultraviolet emission[37,38]. In Fig. 5(d), the ultraviolet light emission intensity of the sample is normalized. Following the introduction of Ta doping, there is a significant increase in the relative luminescence intensity in the visible light region. Moreover, the impact of changes in Ta concentration after doping on the emission intensity in the visible light region is considerably smaller than the impact of the presence of Ta doping itself.

To enhance the analysis of the photoluminescence mechanisms and defect density, Gaussian peak fitting was implemented to deconvolute the PL spectra within the visible light region. Notably, the introduction of Ta does not result in additional peaks in the PL spectra. All sample PL spectra were fitted using peaks centered around wavelengths of approximately 450, 520, 580, 630, and 680 nm, and the second-order diffraction peak changed with NBE, corresponding to blue–purple, blue, green, yellow, orange, and infrared emissions. The purple–blue and blue emission peaks are attributed to transitions from extended zinc interstitials and oxygen vacancies to the valence band maximum (ex-Zn_i → VBM, V_O → VBM)[39–41]. The green and yellow emission peaks mainly originate from transitions from the conduction band minimum and zinc interstitials to oxygen interstitials (CBM → O_i, Zn_i → O_i)[42,43]. The orange emission peak may result from the transition from the conduction band minimum to zinc vacancies (CBM → V_{Zn})[44]. To further quantify the defect density, the integral area ratio of the main defect in the visible light region to the UV region emission peak ($I_{(B,G,Y,O)}/I_{UV}$) was studied[45,46].

By examining the trend of the luminescence intensity ratio between the visible light region and the ultraviolet region, the variation in the defect density was semiquantitatively investigated (refer to Fig. 6). It was observed that pure ZnO films, despite containing intrinsic defects, exhibit a relatively low defect density. With the introduction of Ta, an overall increase in the defect density was noted, a phenomenon associated with a reduction in the grain size and an increase in the degree of film disorder. The increase in luminescence intensity within the blue and green regions signifies the transfer of oxygen in the lattice to interstitial sites with increasing Ta concentration, leading to a simultaneous increase in V_O and O_i defects. The enhanced orange luminescence is associated

with an increase in defects due to crystallinity degradation, and the subsequent decrease with Ta doping may be attributed to Ta occupying zinc vacancies in the lattice sites. Numerous studies have highlighted a close correlation between alterations in carrier concentration and intrinsic defect density in ZnO films[46,47]. In our measured PL spectra, the variation in the defect luminescence intensity in the visible light region cannot fully explain the changes in carrier concentration, indicating the presence of defects that do not contribute to radiative transitions affecting the carrier concentration. Combined with the previous analysis, this may be related to the incorporation of Ta into interstitial or grain boundary sites.

Optical properties

Fig. 7 shows the optical characteristics of the TZO films, where excellent transmission was observed across the visible spectrum for all the samples. With Ta doping, a blueshift in the absorption edge was observed. This shift is attributed to the increase in the TZO bandgap. Since ZnO is a direct bandgap semiconductor, its optical bandgap (E_g) follows the following relationship:

$$(\alpha h\nu)^2 = A(h\nu - E_g), \alpha = \frac{1}{d}\ln\left(\frac{1}{T}\right)$$

where A is a constant, hν is the photon energy, and the absorption coefficient α can be computed from the thickness (d) and transmittance (T) of the films. By plotting $(\alpha h\nu)^2$ as a function of the photon energy (hν) and performing a linear fit, the bandgap can be determined[48]. Furthermore, the first derivative of the transmittance with respect to the photon energy is calculated, as illustrated in Fig. 7. Numerous studies on doped films attribute the broadening of the bandgap to the Burstein–Moss effect[49–53]. The premise is that the electron concentrations in these films exceed the Mott critical density and that the Fermi level is positioned within the conduction band, resulting in the filling of part of the bottom of the conduction band by electrons. Therefore, the Pauli exclusion principle prohibits optical transitions to these states, resulting in optical absorption occurring at higher energy levels, leading to the expansion of the bandgap[54]. At this juncture, in the case of photoluminescence (PL) emission, the states between the bottom of the conduction band and the Fermi level are filled with electrons. These electrons can undergo transitions to the valence band under excitation, leading to radiative emission. Consequently, the PL emission energy values near the band edge of these films are lower than the optical bandgaps[55–57]. Figure 7(d) and Table 1 present the bandgap-related data obtained from Tauc plots, dT/dE, and PL spectra in this experiment. The PL emission energy values near the band edge for all the films exceed the bandgaps obtained from the Tauc plot, which is also documented in other studies on doped ZnO[58,59]. Moreover, the carrier concentration of the films in these two opposite phenomena is distinguished by the Mott critical density in ZnO (approximately 7×10^{19} cm^{-3})[55]. For the films with carrier concentrations below the Mott critical density, the PL emission energy near the band edge is greater than the bandgap obtained from the Tauc plot, which
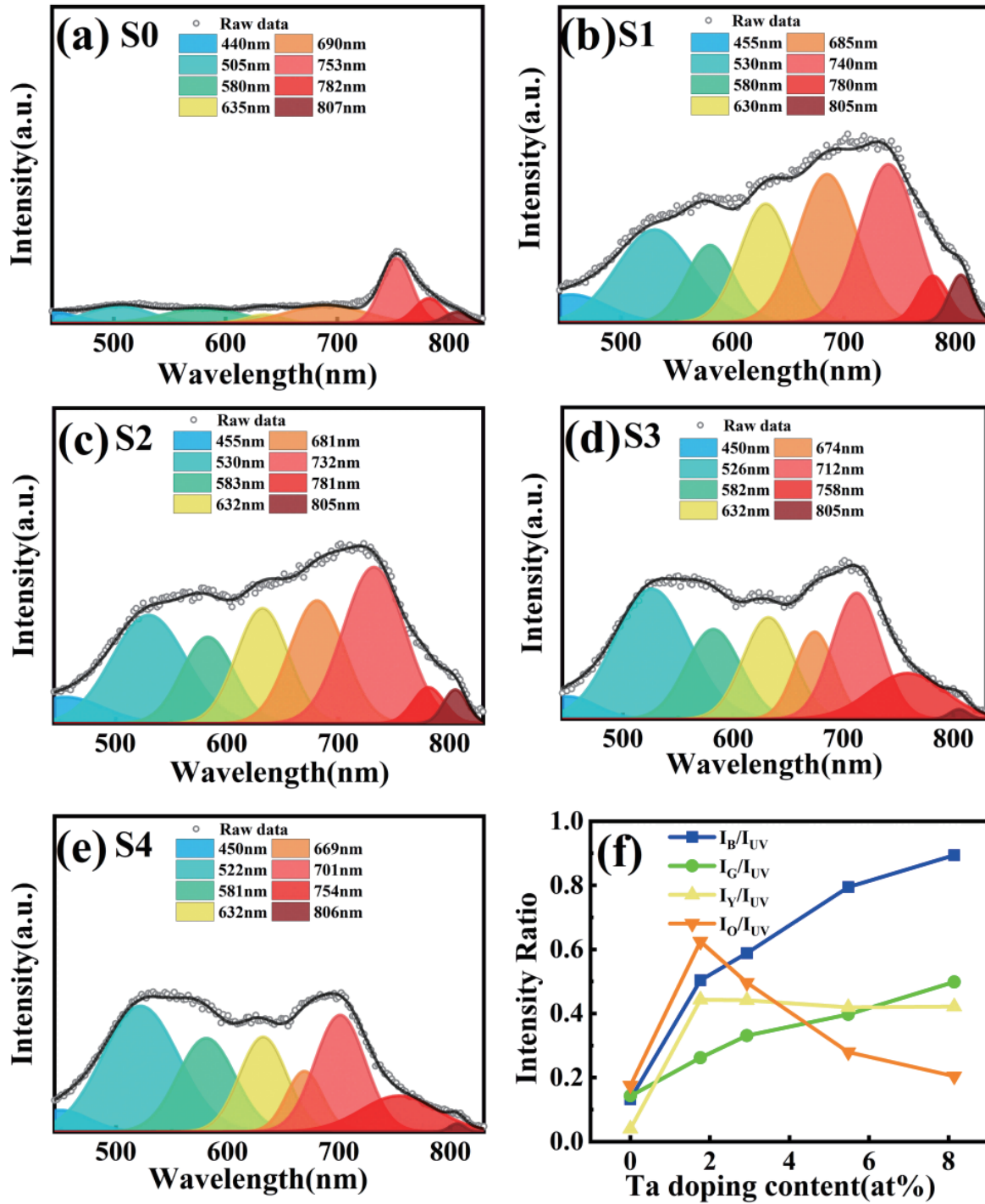
Fig. 6. (a) (b) (c) (d) (e): Gaussian fitting of the visible light region of ZnO films with different Ta contents; (f) intensity ratios of the blue, green, yellow, and orange emission peaks to the UV emission peaks.

is fully consistent with this experiment (see Figure 3(b)). Figure 7(d) shows that the PL emission energy near the band edge of undoped ZnO is lower than the bandgap energy, whereas the energy difference increases after Ta doping. We speculate that this is related to the levels near the conduction band in the bandgap of the films. Undoped ZnO has fewer defect levels, and electron transitions during absorption and emission mainly occur between the bottom of the conduction band (CBM) and the top of the valence band (VBM). After doping, the number of defects increases, and those levels near the conduction band are unoccupied, allowing optical absorption to occur between the VBM and these levels. In the case of PL emission, electron transitions mainly occur between the CBM and VBM.

The derivation of a crystal's band structure is based on first principles, which are accomplished through computing the density of states of each atomic orbital. The band structure of the crystal can be obtained by integrating the density of states
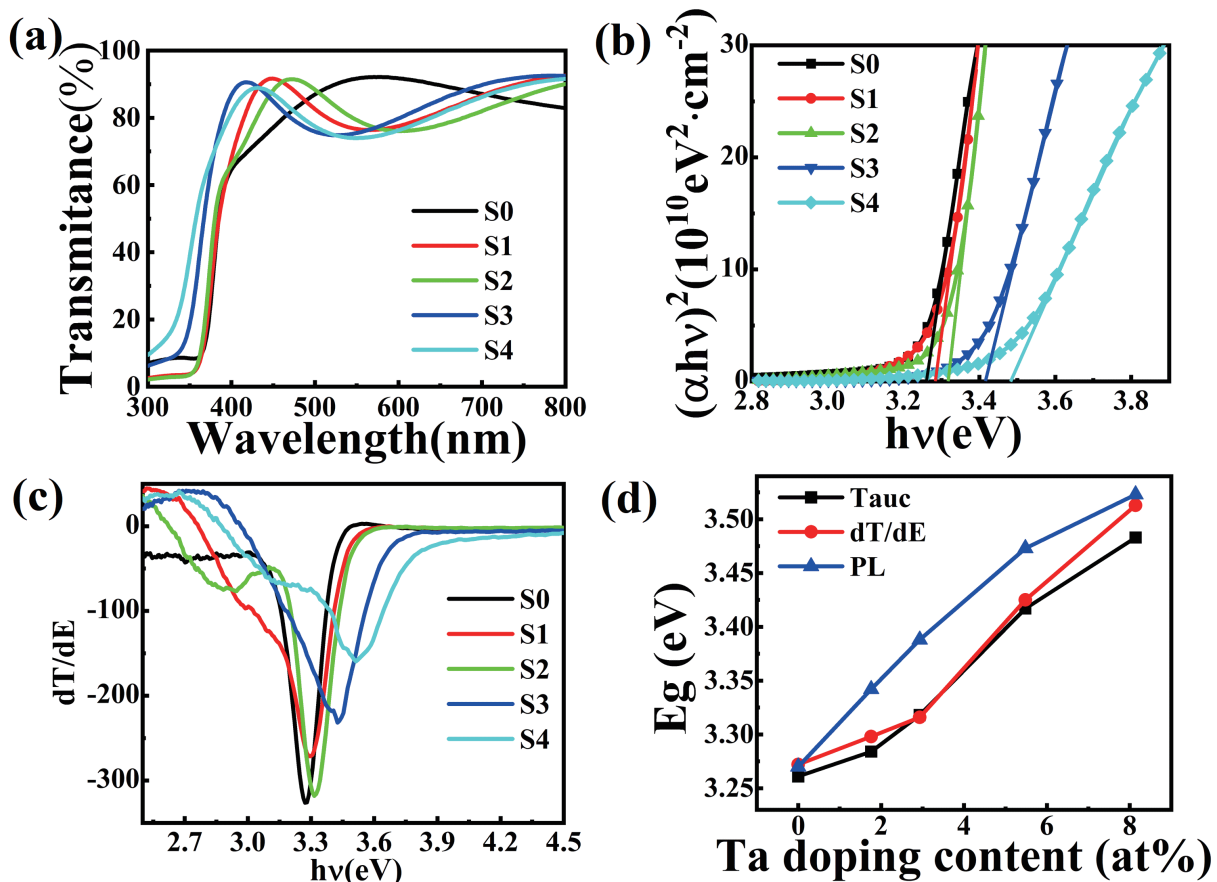
Fig. 7. (a) Ultraviolet–visible transmittance spectra; (b) plot of $(\alpha h\nu)^2$ vs. $h\nu$; (c) plot of dT/dE vs. $h\nu$; (d) band gaps obtained from the Tauc plots, dT/dE plots, and PL spectra.

Table 1. Band gaps of Ta-doped ZnO films obtained from Tauc plots, dT/dE plots, and PL spectra.

Sample	Band gap (eV)		
	Tauc	dT/dE	PL
S0	3.26	3.27	3.27
S1	3.28	3.30	3.34
S2	3.32	3.32	3.39
S3	3.42	3.43	3.47
S4	3.48	3.51	3.52

in space, so any change in the band structure can be explained by the change in the density of states. In the band structure of ZnO, the valence band maximum (VBM) is influenced primarily by O 2p states, whereas the conduction band minimum (CBM) is predominantly determined by Zn 4s states[60]. Turning to the band structure of Ta_2O_5, the VBM relies on O 2p orbitals, with the main contribution to the conduction band originating from Ta 5d orbitals[61]. The electron affinity of Ta_2O_5 (3.14 eV) is smaller than that of ZnO (4.5 eV)[62,63], indicating that the energy position of the Ta 5d states surpasses that of the Zn 4s states. When Ta is doped into ZnO and replaces Zn at lattice sites, coupling between Zn 4s states and Ta 5d states occurs in the conduction band, resulting in an upward shift of CBM. This phenomenon has also been ob-

served in Mg-doped ZnO[64]. The changes in the valence band determined by O 2p states are relatively small, resulting in an expansion of the bandgap. Nevertheless, at high doping concentrations, most of Ta enters interstitial or grain boundaries rather than replacing Zn. In such instances, owing to the deterioration of the film crystallinity, the grain size decreases to less than 10 nm, and the expansion of the bandgap is associated with quantum size effects[65,66].

Conclusion

This experiment systematically investigated the influence of Ta doping on the microstructure and optoelectronic properties of ZnO films. These results indicate that the doping of Ta introduces additional defects and reduces the grain size. The solubility limit of Ta in ZnO is approximately 5–6 at%, beyond which the increase in the number of grain boundaries and defects reduces mobility, resulting in a reduction in the carrier concentration. Upon reaching a doping concentration of 8.1 at%, the carrier concentration in the film decreases to approximately 10^{14} cm^{-3}. The luminescent mechanism of the film was studied through photoluminescence, further confirming the aforementioned conclusions. A comparison of the transmission spectra with the photoluminescence spectra revealed that the difference in the emission and absorption optical transition mechanisms of the doped ZnO films is closely related to whether the Fermi level enters the conduction band.

Additionally, the bandgap of ZnO films is increased by Ta doping, a phenomenon linked to the coupling of Ta and Zn energy levels and quantum size effects. In summary, Ta-doped ZnO films can concurrently modulate the carrier concentration and bandgap, indicating potential applications in specific optoelectronic devices.

Conflict of interest

The authors declare that they have no known competing financial interests or personal relationships that could have appeared to influence the work reported in this paper.

Funding Information

References

[1] Moulahi A, Sediri F. Pencil-like zinc oxide micro/nano-scale structures: Hydrothermal synthesis, optical and photocatalytic properties. *Materials Research Bulletin*, **2013**, *48*: 3723–3728.

[2] Faisal M, Ibrahim A A, Harraz F A, et al. SnO_2 doped ZnO nanostructures for highly efficient photocatalyst. *Journal of Molecular Catalysis A: Chemical*, **2015**, *397*: 19–25.

[3] Amna S, Shahrom M, Azman S, et al. Review on Zinc Oxide Nanoparticles: Antibacterial Activity and Toxicity Mechanism. *Nano-Micro Letters*, **2015**, *7*: 219–242.

[4] Zhu L, Zeng W. Room-temperature gas sensing of ZnO-based gas sensor: A review. *Sensors and Actuators A: Physical*, **2017**, *267* (1): 242–261.

[5] Paul R, Arulkumar S, Jenifer K, et al. Al-Diffused ZnO Transparent Conducting Oxide Thin Films for Cadmium Telluride Superstrate Solar Cells: A Comprehensive Study. *Journal of Electronic Materials*, **2023**, *52*: 130–139.

[6] Mustaqima M, Liu C. ZnO-based nanostructures for diluted magnetic semiconductor. *Turkish Journal of Physics*, **2014**, *38* (3): 429–441.

[7] Chen X X, Yin Z Z, Yan J L, et al. Fabrication of $ZnO@Fe_2O_3$ superhydrophobic coatings with high thermal conductivity. *Surface and Coatings Technology*, **2023**, *467*: 129701.

[8] Yin Z Z, Yuan F, Zhou D P, et al. Ultra dynamic water repellency and anti-icing performance of superhydrophobic ZnO surface on the printed circuit board (PCB). *Chemical Physics Letters*, **2021**, *771*: 138558.

[9] Yin Z Z, Xue M S, Luo Y D, et al. Excellent static and dynamic anti-icing properties of hierarchical structured ZnO superhydrophobic surface on Cu substrates. *Chemical Physics Letters*, **2020**, *755*: 137806.

[10] Zhou T H, Yin Z Z, Chen X X, et al. Mussel-inspired fabrication of superior superhydrophobic cellulose-based composite membrane for efficient oil emulsions separation, excellent anti-microbial property and simultaneous photocatalytic dye degradation. *Separation and Purification Technology*, **2022**, *286*: 120504.

[11] Li M, Yin Z Z, Li Z H, et al. A harsh environment resistant robust $Co(OH)_2$@stearic acid nanocellulose-based membrane for oil-water separation and wastewater purification. *Journal of Environmental Management*, **2023**, *342*: 118127.

[12] Chang G S, Kurmaev E Z, Boukhvalov D W, et al. Co and Al co-doping for ferromagnetism in ZnO: Co diluted magnetic semiconductors. *Journal of Physics: Condensed Matter*, **2009**, *21* (5): 056002.

[13] Ko H J, Chen Y F, Zhu Z, et al. Photoluminescence properties of ZnO epilayers grown on CaF_2(111) by plasma assisted molecular beam epitaxy. *Applied Physics Letters*, **2000**, *76*: 1905–1907.

[14] Belghazi Y, Ait Aouaj M, Yadari M E, et al. Elaboration and characterization of Co-doped ZnO thin films deposited by spray pyrolysis technique. *Microelectronics Journal*, **2009**, *40* (2): 265–267.

[15] Belghazi Y, Schmerber G, Colis S, et al. Room-temperature ferromagnetism in Co-doped ZnO thin films prepared by sol-gel method. *Journal of Magnetism and Magnetic Materials*, **2007**, *310* (2): 2092–2094.

[16] Petersen J, Brimont C, Gallart M, et al. Correlation of structural properties with energy transfer of Eu-doped ZnO thin films prepared by sol-gel process and magnetron reactive sputtering. *Journal of Applied Physics*, **2010**, *107*: 123522.

[17] Deng Y T, Xu F L, Yin Z Z, et al. Controllable fabrication of superhydrophobic alloys surface on 304 stainless steel substrate for anti-icing performance. *Ceramics International*, **2023**, *49* (15): 25135–25143.

[18] Yuan F, Yin Z Z, Xue M S, et al. A multifunctional and environmentally safe superhydrophobic membrane with superior oil/water separation, photocatalytic degradation and anti-biofouling performance. *Journal of Colloid and Interface Science*, **2022**, *611*: 93–104.

[19] Chen X X, Yin Z Z, Chen Z B, et al. Superhydrophobic Photocatalytic Self-Cleaning Nanocellulose-Based Strain Sensor for Full-Range Human Motion Monitoring. *Advanced Materials Interfaces*, **2023**, *10* (33): 2300350.

[20] Janotti A, Van de Walle C G. Native point defects in ZnO. *Physical Review B*, **2007**, *76* (16): 165202.

[21] Yang Y H, Chen X Y, Feng Y, et al. Physical Mechanism of Blue-Shift of UV Luminescence of a Single Pencil-Like ZnO Nanowire. *Nano Letters*, **2007**, *7* (12): 3879–3883.

[22] Mahmood K, Song D, Park S B. Effects of thermal treatment on the characteristics of boron and tantalum-doped ZnO thin films deposited by the electrospraying method at atmospheric pressure. *Surface and Coatings Technology*, **2012**, *206* (23): 4730–4740.

[23] Wu Y H, Li C P, Li M J, et al. Microstructural and optical properties of Ta-doped ZnO films prepared by radio frequency magnetron sputtering. *Ceramics International*, **2016**, *42* (9): 10847–10853.

[24] Cheng Y L, Cao L, He G, et al. Preparation, microstructure and photoelectrical properties of Tantalum-doped zinc oxide transparent conducting films. *Journal of Alloys and Compounds*, **2014**, *608* (25): 85–89.

[25] Liu X, Pan K, Li W B, et al. Optical and gas sensing properties of Al-doped ZnO transparent conducting films prepared by sol-gel method under different heat treatments. *Ceramics International*, **2014**, *40* (7): 9931–9939.

[26] Xu G Q, Shen X K, Hu Y, et al. Fabrication of tantalum oxide layers onto titanium substrates for improved corrosion resistance and cytocompatibility. *Surface and Coatings Technology*, **2015**, *272* (25): 58–65.

[27] Su Y G, Lang J Y, Li L P, et al. Unexpected Catalytic Performance in Silent Tantalum Oxide through Nitridation and Defect Chemistry. *Journal of the American Chemical Society*, **2013**, *135* (31): 11433–11436.

[28] Wang L W, Wu F, Tian D X, et al. Effects of Na content on structural and optical properties of Na-doped ZnO thin films prepared by sol-gel method. *Journal of Alloys and Compounds*, **2015**, *623* (25): 367–373.

[29] Lee J H, Song J T. Dependence of the electrical and optical properties on the bias voltage for ZnO: Al films deposited by r. f. magnetron sputtering. *Thin Solid Films*, **2008**, *516* (7): 1377–1381.

[30] Poongodi G, Kumar R M, Jayavel R. Structural, optical and visible light photocatalytic properties of nanocrystalline Nd doped ZnO thin films prepared by spin coating method. *Ceramics International*, **2015**, *41* (3): 4169–4175.

[31] Lv M S, Xiu X W, Pang Z Y, et al. Structural, electrical and optical

properties of zirconium-doped zinc oxide films prepared by radio frequency magnetron sputtering. *Thin Solid Films*, **2008**, *516* (8): 2017–2021.

[32] Soumahoro I, Colis S, Schmerber G, et al. Structural, optical, spectroscopic and electrical properties of Mo-doped ZnO thin films grown by radio frequency magnetron sputtering. *Thin Solid Films*, **2014**, *566* (1): 61–69.

[33] Toma M, Domokos R, Lung C, et al. Characterization of ZnO, Ga-Doped ZnO, and Nd-Ga-Doped ZnO Thin Films Synthesized by Radiofrequency Magnetron Sputtering. *Analytical Letters*, **2023**.

[34] Ravichandran K, Subha K, Dineshbabu K, et al. Enhancing the electrical parameters of ZnO films deposited using a low-cost chemical spray technique through Ta doping. *Journal of Alloys and Compounds*, **2016**, *656* (25): 332–338.

[35] Nistor M, Mihut L, Millon E, et al. Tailored electric and optical properties of Nd doped ZnO: from transparent conducting oxide to photon down-shifting thin films. *RSC Advances*, **2016**, *6*: 41465–41472.

[36] Janotti A, Van de Walle C G. Fundamentals of zinc oxide as a semiconductor. *Reports on Progress in Physics*, **2009**, *72*: 126501.

[37] Wang Y G, Lau S P, Lee H W, et al. Photoluminescence study of ZnO films prepared by thermal oxidation of Zn metallic films in air. *Journal of Applied Physics*, **2003**, *94*: 354–358.

[38] Lv J G, Liu C L, Gong W B, et al. Temperature-dependent shifts of near band-edge emission and their second-order diffraction for ZnO nanorods. *Optical Materials*, **2012**, *34* (11): 1917–1920.

[39] Wang M S, Zhou Y J, Zhang Y P, et al. Near-infrared photoluminescence from ZnO. *Applied Physics Letters*, **2012**, *100*: 101906.

[40] Kayaci F, Vempati S, Donmez I, et al. Role of zinc interstitials and oxygen vacancies of ZnO in photocatalysis: a bottom-up approach to control defect density. *Nanoscale*, **2014**, *6*: 10224–10234.

[41] Biroju R K, Giri P K. Strong visible and near infrared photoluminescence from ZnO nanorods/nanowires grown on single layer graphene studied using sub-band gap excitation. *Journal of Applied Physics*, **2017**, *122*: 044302.

[42] Wu X L, Siu G G, Fu C L, et al. Photoluminescence and cathodoluminescence studies of stoichiometric and oxygen-deficient ZnO films. *Applied Physics Letters*, **2001**, *78*: 2285–2287.

[43] Kumar V, Swart H C, Ntwaeaborwa O M, et al. Origin of the red emission in zinc oxide nanophosphors. *Materials Letters*, **2013**, *101*: 57–60.

[44] Perkins J, Foster G M, Myer M, et al. Impact of Mg content on native point defects in $Mg_xZn_{1-x}O$ ($0 \leq x \leq 0.56$). *APL Materials*, **2015**, *3*: 062801.

[45] Singha C, Panda E. Variation of electrical properties in thickening Al-doped ZnO films: role of defect chemistry. *RSC Advances*, **2016**, *6*: 48910–48918.

[46] Zhang H, Li W, Qin G P, et al. Role of zinc interstitial defects in indium and magnesium codoped ZnO transparent conducting films. *Applied Surface Science*, **2019**, *492*: 392–398.

[47] Dhawan R, Panda E. Mg addition in undoped and Al-doped ZnO films: Fabricating near UV transparent conductor by bandgap engineering. *Journal of Alloys and Compounds*, **2019**, *788*: 1037–1047.

[48] Ngom B D, Mpahane T, Manyala N, et al. Structural and optical properties of nano-structured tungsten-doped ZnO thin films grown by pulsed laser deposition. *Applied Surface Science*, **2009**, *255* (7):

4153–4158.

[49] Burstein E. Anomalous Optical Absorption Limit in InSb. *Physical Review*, **1954**, *93* (3): 632–633.

[50] Moss T S. The Interpretation of the Properties of Indium Antimonide. *Proceedings of the Physical Society*, **1954**, *67*: 775.

[51] Lu J G, Fujita S, Kawaharamura T, et al. Carrier concentration dependence of band gap shift in n-type ZnO: Al films. *Journal of Applied Physics*, **2007**, *101*: 083705.

[52] Kronenberger A, Polity A, Hofmann D M, et al. Structural, electrical, and optical properties of hydrogen-doped ZnO films. *Physical Review B*, **2012**, *86* (11): 115334.

[53] Liu C, Yuan Y F, Zhang X T, et al. Ta Doping Effect on Structural and Optical Properties of InTe Thin Films. *Nanomaterials*, **2020**, *10* (9): 1887.

[54] Saha D, Misra P, Joshi M P, et al. Investigating Optical Properties of Atomic Layer Deposited ZnO/TiOx Multi-stacked Thin Films Above Mott Critical Density. *The Journal of Physical Chemistry C*, **2017**, *121* (33): 18129–18136.

[55] Makino T, Segawa Y, Yoshida S, et al. Gallium concentration dependence of room-temperature near-band-edge luminescence in n-type ZnO: Ga. *Applied Physics Letters*, **2004**, *85*: 759–761.

[56] Luo J T, Zhu X Y, Chen G, et al. The electrical, optical and magnetic properties of Si-doped ZnO films. *Applied Surface Science*, **2012**, *258* (6): 2177–2181.

[57] Mohanty B C, Yeon D H, Das S N, et al. Unusual near-band-edge photoluminescence at room temperature in heavily-doped ZnO: Al thin films prepared by pulsed laser deposition. *Materials Chemistry and Physics*, **2013**, *140* (2-3): 610–615.

[58] Wu F, Fang L, Pan Y J, et al. Effect of annealing treatment on structural, electrical, and optical properties of Ga-doped ZnO thin films deposited by RF magnetron sputtering. *Thin Solid Films*, **2011**, *520* (2): 703–707.

[59] Zheng Z, Lu Y F, Ye Z Z, et al. Carrier type- and concentration-dependent absorption and photoluminescence of ZnO films doped with different Na contents. *Materials Science in Semiconductor Processing*, **2013**, *16* (3): 647–651.

[60] Guan L, Liu B T, Li Q, et al. Electronic structure and optical properties of substitutional and interstitial phosphor-doped ZnO. *Physics Letters A*, **2011**, *375* (5): 939–945.

[61] Nashed R, Hassan W M I, Ismailc Y, et al. Unravelling the interplay of crystal structure and electronic band structure of tantalum oxide (Ta_2O_5). *Physical Chemistry Chemical Physics*, **2013**, *15*: 1352–1357.

[62] Jacobi K, Zwicker G, Gutmann A. Work function, electron affinity and band bending of zinc oxide surfaces. *Surface Science*, **1984**, *141* (1): 109–125.

[63] Song T S, Cho J W, Kim J H, et al. High ultraviolet transparent conducting electrodes formed using tantalum oxide/Ag multilayer. *Ceramics International*, **2022**, *48* (3): 3536–3543.

[64] Takahashi R, Dazai T, TsukaharaY, et al. Mg substitution effect on the electron affinity of ZnO films. *Journal of Applied Physics*, **2022**, *131*: 175302.

[65] Tan S T, Chen B J, Sun X W, et al. Blueshift of optical band gap in ZnO thin films grown by metal-organic chemical-vapor deposition. *Journal of Applied Physics*, **2005**, *98*: 013505.

[66] Lu J G, Ye Z Z, Zhang Y Z, et al. Self-assembled ZnO quantum dots with tunable optical properties. *Applied Physics Letters*, **2006**, *89*: 023122.